

## Relevant parameter space and stability of spherical tokamaks with a plasma center column

L. G. Lampugnani, P. L. Garcia-Martinez, and R. Farengo

Citation: *Physics of Plasmas* **24**, 022501 (2017); doi: 10.1063/1.4975018

View online: <http://dx.doi.org/10.1063/1.4975018>

View Table of Contents: <http://aip.scitation.org/toc/php/24/2>

Published by the *American Institute of Physics*

---

### Articles you may be interested in

[Electromagnetic electron temperature gradient driven instability in toroidal plasmas](#)

*Physics of Plasmas* **24**, 024501024501 (2017); 10.1063/1.4975189

[Action principles for relativistic extended magnetohydrodynamics: A unified theory of magnetofluid models](#)

*Physics of Plasmas* **24**, 022103022103 (2017); 10.1063/1.4975013


[Nanosecond electrical explosion of bare and dielectric coated tungsten wire in vacuum](#)

*Physics of Plasmas* **24**, 022702022702 (2017); 10.1063/1.4975650

[Observation of the double e-fishbone instability in HL-2A ECRH/ECCD plasmas](#)

*Physics of Plasmas* **24**, 022110022110 (2017); 10.1063/1.4975667

---



Small Conferences. BIG Ideas.

Applied Physics Reviews

SAVE THE DATE!

**3D Bioprinting: Physical and Chemical Processes**

May 2–3, 2017 • Winston Salem, NC, USA

## Relevant parameter space and stability of spherical tokamaks with a plasma center column

L. G. Lampugnani,<sup>1,2,a)</sup> P. L. Garcia-Martinez,<sup>1,3</sup> and R. Farengo<sup>2,3</sup>

<sup>1</sup>*CCT Patagonia Norte (CONICET), 8400 Bariloche, Argentina*

<sup>2</sup>*Instituto Balseiro, UNCuyo, Av. Bustillo 9500, 8400 Bariloche, Argentina*

<sup>3</sup>*Centro Atómico Bariloche (CAB-CNEA), Av. Bustillo 9500, 8400 Bariloche, Argentina*

(Received 19 December 2016; accepted 12 January 2017; published online 7 February 2017)

A spherical tokamak (ST) with a plasma center column (PCC) can be formed inside a simply connected chamber via driven magnetic relaxation. From a practical perspective, the ST-PCC could overcome many difficulties associated with the material center column of the standard ST reactor design. Besides, the ST-PCC concept can be regarded as an advanced helicity injected device that would enable novel experiments on the key physics of magnetic relaxation and reconnection. This is because the concept includes not only a PCC but also a coaxial helicity injector (CHI). This combination implies an improved level of flexibility in the helicity injection scheme required for the formation and sustainment phases. In this work, the parameter space determining the magnetic structure of the ST-PCC equilibria is studied under the assumption of fully relaxed plasmas. In particular, it is shown that the effect of the external bias field of the PCC and the CHI essentially depends on a single parameter that measures the relative amount of flux of these two entities. The effect of plasma elongation on the safety factor profile and the stability to the tilt mode are also analyzed. In the first part of this work, the stability of the system is explained in terms of the minimum energy principle, and relevant stability maps are constructed. While this picture provides an adequate insight into the underlying physics of the instability, it does not include the stabilizing effect of line-tying at the electrodes. In the second part, a dynamical stability analysis of the ST-PCC configurations, including the effect of line-tying, is performed by numerically solving the magnetohydrodynamic equations. A significant stability enhancement is observed when the PCC contains more than the 70% of the total external bias flux, and the elongation is not higher than two.

Published by AIP Publishing. [<http://dx.doi.org/10.1063/1.4975018>]

### I. INTRODUCTION

Spherical torus or tokamak (ST) plasmas are toroidal confinement configurations with a very small aspect ratio. It has been demonstrated that they have a number of attractive physical features, such as a high  $\beta$  limit and a low geodesic curvature of the magnetic field lines. From the perspective of a fusion reactor, the low aspect ratio implies the possibility of compact fusion at low field and modest cost.<sup>1,2</sup> In conventional spherical tokamaks, the plasma torus is linked by a central post containing the inner part of the toroidal magnet and the ohmic transformer. Due to the very limited space left at the low aspect ratio, the design of this centerpost becomes a very difficult challenge. Another problem is that the centerpost cannot be shielded from the neutron flux and therefore cannot be a superconductor.

To overcome these limitations, it has been proposed to replace the center-post by a pair of electrodes linked by open flux surfaces across the plasma center.<sup>3,4</sup> Biasing these electrodes, a poloidal current may be driven along the open flux surfaces to produce the toroidal magnetic field. With this approach, configurations with many features in common with spherical tokamaks could be formed and sustained inside simply connected chambers. The first and simplest

configuration using this idea is the flux-core spheromak (FCS),<sup>5</sup> although in this configuration much of the toroidal field is produced by currents flowing in the closed flux region. A more advanced proposal is the Proto-Sphera experiment,<sup>3</sup> which involves a central screw-pinch fed by electrodes and surrounded by a spherical torus.

Another configuration of this type is the spherical tokamak with plasma center column (ST-PCC).<sup>4,6</sup> This configuration can be naturally formed by driven relaxation inside a cylindrical flux conserver. The required injection of magnetic helicity is provided by the PCC along with a coaxial helicity injector (CHI). In this sense, the ST-PCC may be regarded as a combination of a FCS and a conventional gun spheromak.<sup>7-9</sup> Tang and Boozer<sup>4</sup> studied these configurations under the assumption of complete relaxation<sup>5,10</sup> and showed that their magnetic structure is primarily determined by four factors: (1) the flux amplification factor [see Eq. (4)], (2) the elongation of the cylinder, (3) the requirement of stability to the tilt mode, and (4) the vacuum bias flux imposed by a set of electrodes.

In this paper, we study the relaxed states of ST-PCC configurations. The first important result is the demonstration that the analysis of these configurations can be greatly simplified by noting that the effect of the vacuum bias flux on the equilibrium essentially depends on a single quantity:  $f$ , the normalized magnetic flux content of the PCC (see Sec. II and Fig. 1). This observation allowed us to identify the

<sup>a)</sup>Electronic mail: lealamp@cab.cnea.gov.ar

relevant parameter space of ST-PCC plasmas as  $(e, \lambda, \text{ and } f)$ , where  $e$  is the elongation, and  $\lambda$  is the normalized parallel current [see Eq. (1)]. The role of each parameter is clearly displayed in the mathematical statement of the equilibrium [Eq. (3)]. Furthermore, we cast a theoretical stability condition (to the tilt mode) based on the minimum energy principle<sup>4,11,12</sup> into a stability map, which relates the amplification factor and the stability of the configuration to the control parameters in an intuitive way. We note that the effect of line-tying at the electrodes is not considered by this simplified stability criterion. Notwithstanding, this effect is taken into account in the dynamic stability analysis performed in the second part of this work, as described below. The extreme values of the main figures of merit, such as the safety factor, of the configurations lying on the stable region are given.

Fully relaxed configurations provide a reasonable approximation to the actual ST-PCC equilibria. In fact, they play an important role because the initial formation sequence by driven relaxation is expected to leave the system very close to the fully relaxed state.<sup>4</sup> Moreover, deviations from this state during sustainment will provide a free energy to feed instabilities that, in case of being triggered, will cause the plasma to relax back again. An additional motivation to focus on these preferred states as a starting point is to facilitate the comparison of our results with the existing data on equilibria and stability.<sup>4,11,12</sup>

The sustainment phase of the proposed ST-PCC experiment aims to ramp up the plasma pressure towards conventional high- $\beta$  equilibria with tokamak-like safety factor profiles. Since these scenarios necessarily involve deviations from the relaxed state, the requirement of auxiliary current drive and heating such as rf and neutral beam injection is foreseen.<sup>4,6</sup> The operating conditions must be carefully selected in order to avoid deleterious modes (in particular, due to the absence of a material center column). In order to study the stability as well as the dynamics of magnetohydrodynamic (MHD) modes in these scenarios, the development of a reliable non-linear MHD code is required.

In the second part of this work, a dynamical stability analysis of the tilt mode in ST-PCC configurations is performed using a non-linear MHD code. As a first validation step, the evolution of isolated configurations (i.e., without external bias flux) is computed for different elongations. The theoretical threshold to the tilt mode, as well as the growth rates of the unstable cases previously obtained with linearized codes,<sup>11,12</sup> is correctly reproduced. Next, the stability of relaxed ST-PCC configurations including the external bias is studied. Several sets of runs are used to identify the stability boundaries predicted by the non-linear scheme for different elongations. The results are consistent with the theoretical stability criterion based on the minimum energy principle. In this case, however, the stability thresholds are higher due to the field line-tying at the electrodes, which is not considered by the theoretical criterion. This effect, not considered in previous works,<sup>4,6</sup> produces a significant stability enhancement for configurations with  $e = 2$  and  $f$  in the range 0.7–0.9 but becomes less important for higher elongations and smaller values of  $f$ .

The use of a non-linear MHD code in the present work is considered as a desirable validation step in view of future studies of more complicated phenomena in this kind of configurations. We note that the same numerical scheme was successfully used in previous works to study the current driven instabilities (kink modes)<sup>13–15</sup> as well as the dynamics of formation and sustainment<sup>16,17</sup> of spheromak configurations.

The rest of the paper is organized into three parts. First, in Sec. II, the ST-PCC concept is described in more detail (Sec. II A). The required background on the relaxation theory as well as the mathematical statement of the problem are given (Sec. II B). The role of the relevant control parameters and the construction of stability maps are explained (Secs. II C and II D). The expected safety factor profiles within the stable region are also presented (Sec. II E). Second, in Sec. III, a dynamical stability analysis of the tilt is performed. The MHD model and the numerical scheme employed are described (Sec. III A). Isolated configurations are studied as a preliminary validation step (Sec. III B). The analysis of ST-PCC equilibria including the external bias flux and the effect of line-tying at the electrodes is performed (Sec. III C). Finally, in Sec. IV, the concluding remarks are summarized.

## II. SPHERICAL TOKAMAK WITH PLASMA CENTER COLUMN

### A. Description of the configuration

The ST-PCC concept, proposed by Tang and Boozer,<sup>4</sup> combines a PCC, which is essentially a screw pinch plasma, with a coaxial helicity injector (CHI) to form a toroidal pinch (or ST) via driven relaxation. Fig. 1 shows the flux conserver, the set up of electrodes, and the magnetic field lines of these three magnetic structures.

In order to begin the formation sequence, the open bias flux must be set. The external magnetic flux enters through the central electrode at the bottom ( $\psi_0$ ). A fraction  $f$  of it leaves the chamber through the central electrode at the top

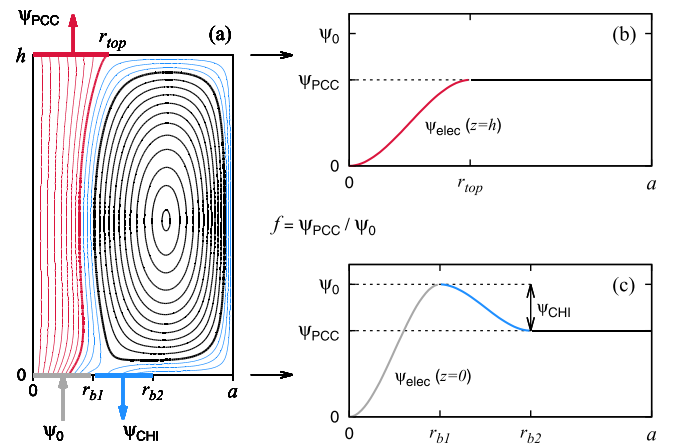


FIG. 1. Magnetic flux surfaces of a typical ST-PCC configuration (a). The PCC is formed by the flux connecting the central electrodes (red lines). The CHI flux links the two concentric electrodes at the bottom (blue lines). The ST composed by closed field lines is formed by driven relaxation (black lines). The distribution of flux across the top (b) and bottom (c) ends of the chamber is also shown.

(the PCC flux,  $\psi_{\text{PCC}}$ ), and the rest leaves the chamber through the outboard electrode at the bottom (the CHI flux,  $\psi_{\text{CHI}}$ ). Note that the possibility of varying the value of  $f$  is a first degree of freedom of this configuration.

The configuration is formed by driven relaxation. In the present scheme, this is accomplished by driving current along the open bias field lines. This produces a build up of magnetic helicity, and a  $j_{\parallel}/B$  gradient is established. Eventually, the system becomes globally unstable, and the relaxation process is triggered. During this process, the magnetic energy is rapidly dissipated, while the magnetic helicity remains approximately constant. As a result, the plasma adopts a preferred state of minimum energy, or relaxed state. There is a large amount of experimental,<sup>8,18–20</sup> theoretical,<sup>5,10</sup> as well as numerical<sup>16,21</sup> work supporting and describing this self-organization mechanism.

After the initial formation stage, the relaxed plasma has low  $\beta$  and a flat  $j_{\parallel}/B$  profile. In this situation, the  $q$  profile typically has reversed shear (i.e.,  $q$  is maximum at the magnetic axis). The sustainment phase aims to ramp up the plasma pressure towards a conventional high- $\beta$  equilibrium with a tokamak like  $q$  profile. The operating conditions of the PCC must be carefully designed in order to achieve these scenarios without triggering the external MHD modes (due to the absence of a material center column). The CHI provides, at this stage, an additional actuator system to drive (either increase or reduce) the parallel current near the separatrix. This may be useful to modify (control) the  $q$  profile or act on the stability of the system (the PCC modes for instance).

While the helicity injection from a single CHI has proven to be a robust method not only for the formation but also for the sustainment of related configurations,<sup>7–9</sup> the requirement of auxiliary current drive and heating schemes, such as rf and neutral beam injection, is foreseen in order to achieve high temperatures and good particle confinement.<sup>4,6</sup> This is because the current drive by helicity injection relies on the tendency of the plasma to relax, and this necessarily involves MHD fluctuations that could degrade the confinement. However, we note that this is a highly non-linear process, and the dynamics of the fluctuations is very sensitive to the operation regime;<sup>17</sup> thus, it is not clear what steady or quasi-steady conditions could achieve in ST-PCC configurations sustained by helicity injection. Moreover, the capability of independently biasing the PCC and CHI provides an improved level of control compared to previous helicity injection experiments. This brings about interesting possibilities of novel research on the dynamics of magnetic relaxation, which is a largely open issue of practical as well as fundamental interest.

## B. Relaxed states and mathematical statement

After the formation phase, the plasma is left in a relaxed state. During the subsequent sustainment phase, departures from this state will provide free energy for potential instabilities which, in case of being triggered, would cause the plasma to relax back again. It is clear then that these

preferred states play a key role, and a deep understanding of their properties is required.

Relaxed states are a special case of force-free plasmas: those for which the ratio between the current and the magnetic field is spatially uniform. This is expressed by the relation

$$\nabla \times \mathbf{B} = \lambda \mathbf{B}, \quad (1)$$

with  $\lambda$  being a constant. The fundamental *ansatz* of relaxation theory is that localized magnetic reconnection events dissipate energy but preserve the global magnetic helicity. Therefore, turbulent fluctuations make the plasma evolve toward the minimum energy state compatible with the initial amount of magnetic helicity.<sup>10</sup> The minimization of the magnetic energy under the constraint of magnetic helicity conservation leads to the linear force-free field (1).<sup>22</sup>

When applied to a simply connected domain with homogeneous boundary conditions, i.e.,  $\mathbf{B} \cdot \mathbf{n} = 0$ , Eq. (1) leads to an eigenvalue problem with a non trivial solution for a discrete set of eigenvalues  $k_i$ . For a magnetic field satisfying Eq. (1), it is easy to verify that

$$\lambda = 2 \frac{W}{K}, \quad (2)$$

where  $W$  is the magnetic energy and  $K$  is the magnetic helicity. Thus, the plasma will tend to evolve toward the minimum allowed  $\lambda$  (the lowest eigenvalue in the homogeneous case). Actual helicity injected devices typically involve electrodes intercepted by the magnetic flux thus,  $\mathbf{B} \cdot \mathbf{n} \neq 0$  at the boundary. In this case, Eq. (1) has a unique solution for any value of  $\lambda$ , excluding the eigenvalues, where there is a resonant behavior. Moreover, it has been shown that Eq. (2) can be extended to open configurations using a gauge invariant definition of the helicity.<sup>5,23</sup>

Since we are interested in axisymmetric configurations, it is convenient to express the condition (1) as a Grad-Shafranov equation for the poloidal flux  $\psi$ . In this way, the relaxed states corresponding to the ST-PCC configurations studied in this work are specified by the following mathematical problem

$$\begin{cases} \Delta^* \psi + \lambda^2 \psi = 0, & \text{on } \Omega = (r, z) \in [0, 1] \times [0, e], \\ \psi = \psi_{\text{elec},f} & \text{on } \partial\Omega, \end{cases} \quad (3)$$

where  $\Delta^* \equiv \partial^2/\partial r^2 - (1/r)\partial/\partial r + \partial^2/\partial z^2$  is the Grad-Shafranov operator and  $\psi_{\text{elec},f}$  is a function defined on the boundary that specifies the flux distribution across the electrodes. All quantities are nondimensionalized using the radius of the flux conserver,  $a$  and the open bias flux  $\psi_0$ , i.e., the flux entering through the central electrode at the bottom. The role of the three control parameters is clearly highlighted in Eq. (3). In particular,  $\lambda$  modifies the governing equation,  $f$  determines the boundary condition, and the elongation ( $e = h/a$ ) sets the geometry of the domain. In Secs. II C-E and III, we analyze the different configurations that can be obtained by

varying these parameters. The stability boundaries on the relevant parameter space will also be identified.

### C. Relevant parameter space

In this section, the choice of the set  $\{\lambda, f, e\}$  as the relevant parameter space defining the relaxed states of the ST-PCC configuration is explained. To begin, we note that  $\lambda$  gives the spatially uniform normalized parallel current  $j_{\parallel}/B$ , as is clear from Eq. (1). The problem defined by Eq. (3) has inhomogeneous boundary conditions and thus has a unique solution for every  $\lambda \neq k_i$ , where  $k_i$  are the eigenvalues of the Grad-Shafranov operator in the rectangle  $\Omega$ . For the study of ST-PCC plasmas, we restrict our attention to the so-called regular configurations, i.e., those below the first resonance. This is expressed as  $\lambda < k_1$ , where  $k_1$  is the lowest eigenvalue. In this case, the solution  $\psi$  is a monotonic function whose maximum gives the magnetic axis.

An important figure for merit of this kind of configurations is the amplification factor, defined as

$$\mathcal{A} = \frac{\psi_{\text{m.a.}}}{\psi_0}, \quad (4)$$

that is, the normalized poloidal flux at the magnetic axis. It is a measure of the effectiveness of a helicity injection scheme since the poloidal flux in the closed flux region is proportional to the toroidal current, which is self-generated by the relaxation process. Note that  $\psi_{\text{m.a.}}$  includes the open as well as the closed fluxes. This means that  $\mathcal{A} > 1$  implies the formation of a closed flux region (the toroidal pinch). For  $\mathcal{A} = 2$ , the amount of poloidal flux enclosed by the toroidal pinch is equal to the external bias flux.

As  $\lambda$  approaches  $k_1$ , the amplification factor diverges. This is shown in Fig. 2 for different values of  $f$ . Note that if  $f$  is set to zero, the configuration reduces to the standard CHI spheromak. On the other hand, by setting  $f=1$ , one recovers the flux core spheromak (FCS) configuration.<sup>5</sup>

The function  $\psi_{\text{elec},f}$  in Eq. (3), specifies the flux distribution across the electrodes. This function must be zero at the axis of symmetry ( $r=0$ ) and equal to  $f$  at the wall ( $r=a$ ). At the base, the (normalized) flux increases up to one at  $r_{b1}$ ,

decreases to  $f$  at  $r_{b2}$ , and then remains constant, as shown in Fig. 1(c). At the top,  $\psi_{\text{elec},f}$  increases up to  $f$  at  $r_{\text{top}}$  and then remains constant, as shown in Fig. 1(b). In principle, one should consider not only  $f$  but also  $r_{b1}$ ,  $r_{b2}$ , and  $r_{\text{top}}$  as the parameters defining the boundary condition.

It turns out, however, that the size of the electrodes plays only a minor role. This is shown in Fig. 2. By changing  $f$ , configurations with very different amplification factors are obtained for each  $\lambda$  (solid curves). On the other hand, if  $f$  is held fixed (equal to 0.5) while  $\{r_{b1}, r_{b2}, r_{\text{top}}\}$  are varied over a large interval, the gray region is obtained. The upper limit of this region corresponds to the ‘‘concentrated electrode’’ configuration,  $r_{b1} = r_{\text{top}} = 0.1$  and  $r_{b2} = 0.2$ , while the lower limit is obtained for  $r_{b1} = 0.9$  and  $r_{b2} = r_{\text{top}} = 1$ . The solid lines correspond to  $r_{b1} = r_{\text{top}} = 0.4$  and  $r_{b2} = 1$ . This choice is used in the rest of the paper. We verified that the effect of the flux distribution across the electrodes is also weak when compared with the effect of changing the fraction of flux of the PCC. All these reasons led us to choose  $f$  as the relevant parameter defining the boundary condition.

Once the electrodes are magnetized, and the value of  $f$  is set, different amounts of current can be driven along the open flux, resulting in different values of  $\lambda$  (assumed to remain spatially uniform due to complete relaxation). Using the same device, i.e., the same flux conserver and electrodes, different values of  $\lambda$  and  $f$  can be explored. In this sense,  $(\lambda, f)$  can be regarded as the set of *operation* parameters. In Fig. 2, it is clear that a given amplification factor can be obtained for different combinations of  $\lambda$  and  $f$ . This clearly shows one of the additional degrees of freedom of the ST-PCC configuration when compared with the conventional CHI spheromak or the FCS.

The remaining relevant parameter defining the ST-PCC relaxed state is the elongation, which appears in the definition of the domain. Physically, the geometry of the plasma container must be changed in order to vary  $e$ . For this reason,  $e$  is regarded as a *design* parameter. The effect of this parameter is worth studying because it is possible to achieve relatively large values of the safety factor with low toroidal fields at high elongations.<sup>4</sup> However, it is well known that elongation is connected to the tilt instability in simply connected configurations.<sup>11,12</sup> In Sec. IID the stability of elongated configurations is discussed in terms of the minimum energy principle.

### D. The tilt mode and the stability map

Relaxed states are quite robust against ideal MHD modes because they are minimum energy states, therefore, any perturbation results in a positive  $\delta W$ .<sup>5,24</sup> This is not surprising, since they have zero  $\beta$  and a uniform  $j_{\parallel}/B$  distribution, and thus the two main ideal instability drivings are absent. Still, the configurations described by Eq. (3) may exhibit a tendency to tilt if the elongation is high enough. This may be understood in terms of the energy minimization principle as follows.<sup>4</sup>

Consider Eq. (1) inside a cylinder with the vanishing normal magnetic field at the boundary. We already mentioned that this problem has non-trivial solutions for a

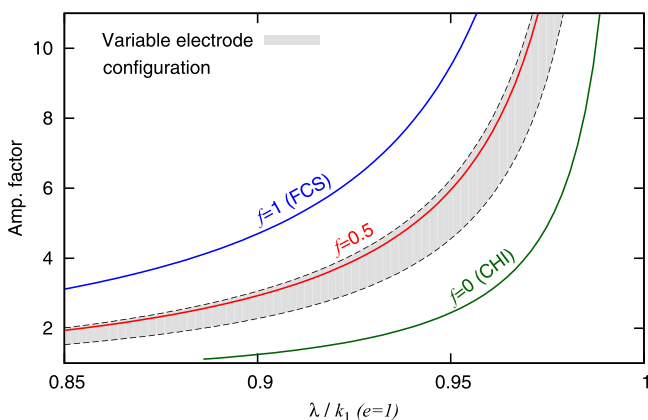


FIG. 2. Flux amplification factor versus  $\lambda$  (normalized with  $k_1$ ) for  $e=1$  and different values of  $f$ . For  $f=0.5$ , the effect of varying the electrode configuration is indicated by the gray region.

discrete set of eigenvalues  $k_i$ , the lowest of which gives the minimum energy eigenstate, i.e., the relaxed state. At this point, it is important to stress that this set of eigenstates includes axisymmetric as well as non-axisymmetric solutions (the Chandrasekhar-Kendall functions<sup>25</sup>). Let us assume that  $k_1$  is the lowest eigenvalue of the axisymmetric ( $n=0$ ) family of eigenstates and that  $k_1^{n=1}$  is the lowest eigenvalue of the non-axisymmetric eigenstates. It turns out that  $k_1 < k_1^{n=1}$  as long as  $e < 1.67$ . For higher elongations, the solution with toroidal mode number  $n=1$  becomes the minimum energy state. In that case, the plasma exhibits the tendency to “tilt.”<sup>11,12</sup>

This result can be used to estimate the threshold of the tilt mode for the configurations defined by Eq. (3). Since we deal with non-homogeneous boundary conditions, the system has a resonance at  $k_1$ , and  $\lambda$  must remain below that resonance in order to have a regular configuration. When  $e > 1.67$ ,  $k_1^{n=1}$  falls below the first resonance predicted by Eq. (3), which only captures the axisymmetric solutions. In these highly elongated cases, one can still avoid the growth of the tilt instability by keeping the operation parameter  $\lambda$  below  $k_1^{n=1}$ . Therefore, the tilt stability threshold can be simply stated as  $\lambda = k_1^{n=1}$ . We note, however, that  $k_1^{n=1}$  represents the onset of the tilt instability for isolated configurations (i.e., without the external flux), and thus, this criterion does not include the stabilizing effect of line-tying at the electrodes. This effect is considered in the dynamical stability analysis presented in Sec. III.

This situation is shown in Fig. 3, where the amplification factor is plotted against  $\lambda$  for  $e=2$  and different values of  $f$ . Our numerical solution of Eq. (3) recovers the theoretical position of the axisymmetric resonance,  $k_1(e=2) = (x_{11}^2 + \pi^2/e^2)^{1/2} = 4.14$ , where  $x_{11}$  is the first zero of the  $J_1$  Bessel function. The tilt stability threshold is  $k_1^{n=1}(e=2) = 3.97$ ,<sup>11,12</sup> above which, the curves are shown with dashed lines. Note that even at  $e=2$ , which is above the theoretical threshold for closed configurations, tilt stable configurations can be obtained for suitable combinations of  $\lambda$  and  $f$ , as indicated by the shaded region.

Taking the pair  $(\lambda, f)$  as the operation parameters, the red region in Fig. 3 may be regarded as the region of stable operation (or stable relaxed states) for  $e=2$ . This region of

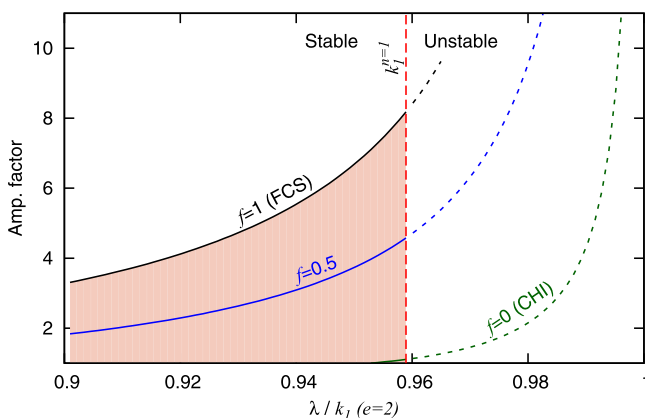


FIG. 3. Amplification factor versus  $\lambda$  for  $e=2$  and different values of  $f$ . Solutions with  $\lambda > k_1^{n=1}$  (dashed lines) are unstable to the tilt mode. The region of stable solutions is shaded in light red.

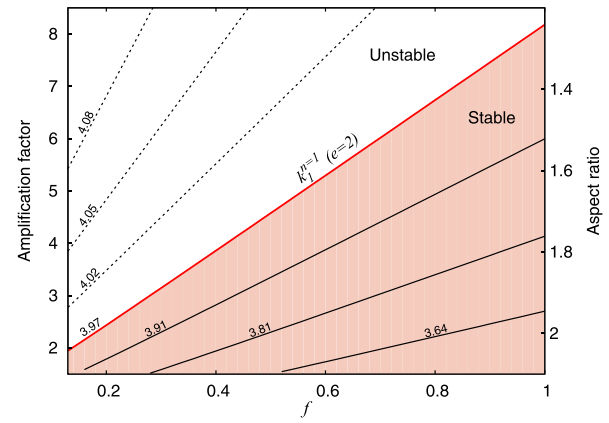


FIG. 4. Stability map for ST-PCC equilibria with  $e=2$ . Contours of constant  $\lambda$  are plotted with solid (dashed) lines in the stable (unstable) region.

stability, or operation range, can also be displayed by plotting the amplification factor against  $f$ , as shown in Fig. 4. Once  $f$  is set, by choosing the fraction of flux carried by the PCC, the flux of the closed configuration can be increased by raising the parallel current, i.e., by increasing  $\lambda$ . The ramp up in  $\lambda$  produces an increase of  $\mathcal{A}$ . The maximum amplification factor achievable for each  $f$  can be directly deduced from this stability map.

As already observed in Figs. 2 and 3, for a fixed  $\lambda$ ,  $f$  has a strong effect on  $\mathcal{A}$ . In Fig. 4, this effect is clearly shown by the contours of  $\lambda$ . Although these contours look like straight lines, they have a very small curvature. The first conclusion we can draw is that increasing the flux of the PCC improves the stability to the tilt:  $\lambda$  can be reduced by increasing  $f$ , and thus, the configuration can be moved away from the stability threshold. In this sense, high values of  $f$  are preferable. We note, however, that in the limit  $f=1$  (FCS), helicity can only be injected using the PCC, and therefore, we lose one of the main advantages of the present configuration, the possibility of independent control of the “external” toroidal field and the helicity injection rate.

In Fig. 5, the tilt stability boundary for configurations with different elongations is shown. As in Fig. 4, stable equilibria for each case lie below the corresponding threshold in

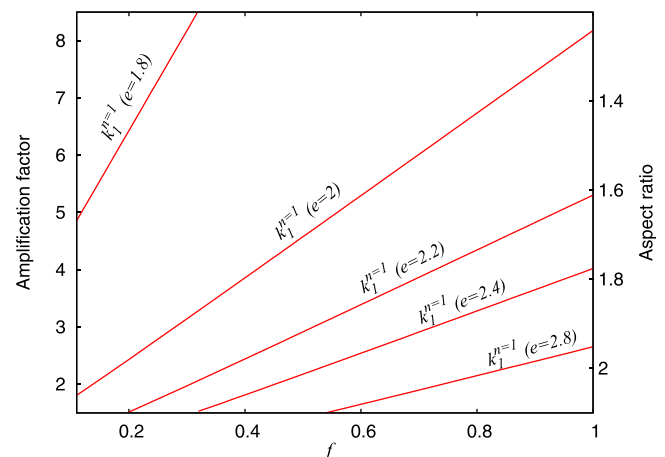


FIG. 5. Stability boundary for configurations with different elongations. As in Fig. 4, stable equilibria lie below the threshold.

an almost triangular region. A second important conclusion drawn from these stability maps is that the region of stable equilibria shrinks rapidly with the elongation. In this sense, configurations with  $e > 2.4$  are, in principle, of limited practical interest.

Another important property of a toroidal confinement configuration is the aspect ratio (the ratio of major to minor radius). As already noted,<sup>4</sup> the aspect ratio scales approximately inversely proportional to the amplification factor and has only a weak dependence on the other parameters of the configuration. Taking advantage of this fact, the aspect ratio has been incorporated on the right y-axis scale of the stability maps in Figs. 4 and 5.

### E. Safety factor profile

The safety factor  $q$  is a fundamental figure of merit closely related to the stability of different types of modes, in particular, current driven modes. At each flux surface,  $q$  gives the number of toroidal turns that a field line completes after one poloidal circuit. Clearly, this quantity depends on the local value of the normalized parallel current  $\lambda$ . It turns out that the parameters  $e$  and  $f$  also have an effect on the  $q$  profile because they affect the geometry of the flux surfaces, which in turn affect the field line trajectories.

The  $q$  profiles obtained for the configurations at three points of the region of stability of Fig. 5 are shown in Fig. 6 for  $e = 2$  and  $e = 2.4$ . The label of each point is indicated in the inset at the upper-left corner of Fig. 6(a). The first point (1), corresponds to  $\lambda = k_1^{n=1}$  and  $f = 1$ , i.e., the marginally stable configuration having the largest  $\mathcal{A}$ . The second point (2) is at  $\lambda = k_1^{n=1}$  and  $\mathcal{A} = 2$ . Finally, the third point (3) is at  $f = 1$  and  $\mathcal{A} = 2$ , which has the lowest  $\lambda$  among these three cases. Note that (1) and (2) have the same  $\lambda$ , (1) and (3) have the same  $f$ , and (2) and (3) have the same  $\mathcal{A}$ .

As is common for relaxed plasmas, the configurations have a central reversed magnetic shear, in the usual tokamak sense. At low amplification factors, the interaction with the open bias results in an increase of  $q$  near the separatrix ( $q_{edge}$ ), producing a region of regular magnetic shear.<sup>4</sup> It is also observed that an increase in  $\lambda$  decreases the central  $q$  (and viceversa). This is in agreement with the basic behavior in tokamaks: for an imposed toroidal field, the central  $q$  drops as the toroidal current becomes peaked (i.e., as the central  $\lambda$  is increased).

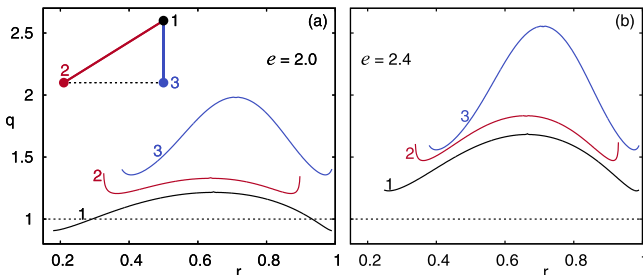


FIG. 6. Safety factor profiles at three points of the stability region for two different elongations. Since quantities vary smoothly inside this region, intermediate profiles may be qualitatively inferred.

An important goal in the proposal of the ST-PCC configuration,<sup>4</sup> as well as the Proto-Sphera experiment,<sup>3</sup> is to produce magnetic equilibria with tokamak like  $q$  profiles inside a simply connected chamber. Since fully relaxed states tend to have flat or reversed  $q$  profiles, as observed in Fig. 6, the sustainment phase will necessarily involve non-uniform distributions of  $\lambda$  (along with a non-zero  $j_{\perp}$  in order to have a finite  $\beta$ ). Despite these unavoidable deviations, relaxed states with a high  $q_{edge}$  would in principle help to achieve the target configurations with regular shear and improved stability.

In Fig. 7,  $q_{edge}$  is shown as a function of the amplification factor for different elongations. As already observed in Fig. 6,  $q$  increases with an elongation and decreases with  $\mathcal{A}$ . Note that several values of  $q_{edge}$  can be obtained for each  $\mathcal{A}$ , since different combinations of  $\lambda$  and  $f$  are possible in the stable region. For this reason, two curves are plotted for each elongation, one corresponds to  $\lambda = k_1^{n=1}$  (the stability threshold) and the other to  $f = 1$  (the FCS limit). Despite this freedom, it turns out that  $q_{edge}$  is essentially determined by  $e$  and  $\mathcal{A}$  and has only a weak dependence on the other parameters.

As observed in Fig. 6,  $q_{edge}$  increases faster than the minimum  $q$ , as the amplification factor decreases. This gives rise to a small region of regular shear and a local minimum in the  $q$  profile. This can also be observed in Fig. 7 where the minimum  $q$  for the marginally stable configurations is shown with dashed lines. This effect only becomes noticeable for  $\mathcal{A} < 4$ .

Finally, Fig. 8 summarizes the maximum  $\mathcal{A}$  and the range of  $q_{edge}$  (dashed lines) that can be obtained for different elongations. The upper  $q_{edge}$  limit is arbitrarily set to  $\mathcal{A} = 2$  (as much closed flux as externally imposed flux) while the lower limit corresponds to the tilt stability boundary (without line-tying).

## III. DYNAMICAL STABILITY ANALYSIS

### A. MHD model and numerical methods

The stability of the configurations described in Sec. II is studied by solving the MHD equations as a time dependent

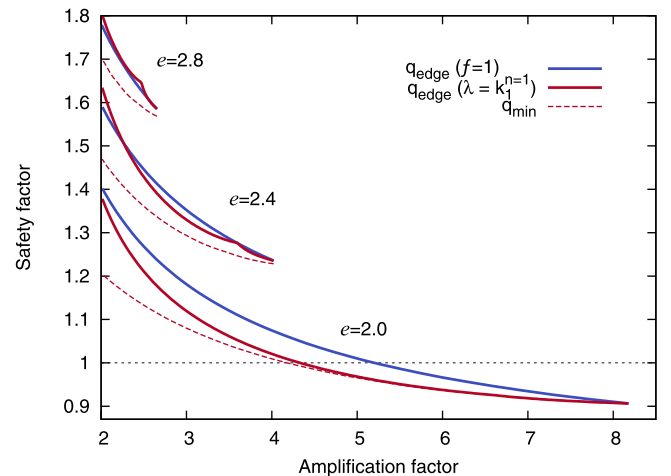


FIG. 7. Safety factor at the separatrix as a function of the amplification factor, for different elongations. Values correspond to the marginal stable states with  $\lambda = k_1^{n=1}$  (red) and the FCS limit  $f = 1$  (blue). The minimum  $q$  for the marginally stable configurations is shown with dashed lines.

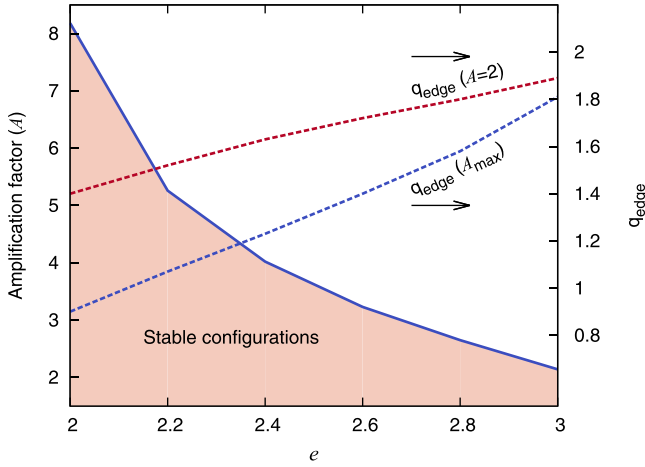


FIG. 8. Flux amplification factor range of stable relaxed states as a function of elongation. The values of  $q$  at the separatrix on the limits of the range are also shown.

problem in three spatial dimensions. The MHD code employed is based on the Versatile Advection Code (VAC)<sup>26</sup> and has already been used to study the dynamics of magnetic relaxation and the helicity injection in spheromak configurations.<sup>13–17,27</sup> In this work, the full MHD equations in the zero  $\beta$  limit are used. The dimensionless form of these equations is

$$\begin{aligned} \frac{\partial \mathbf{u}}{\partial t} + (\mathbf{u} \cdot \nabla) \mathbf{u} &= \frac{1}{\rho_0} (\mathbf{J} \times \mathbf{B}) + \frac{1}{Re} \nabla \Pi, \\ \frac{\partial \mathbf{B}}{\partial t} &= -\nabla \times \mathbf{E}, \\ \mathbf{E} &= -(\mathbf{u} \times \mathbf{B}) + \frac{1}{Re_m} \mathbf{J}, \\ \mathbf{J} &= \nabla \times \mathbf{B}, \\ \nabla \cdot \mathbf{B} &= 0, \end{aligned} \quad (5)$$

where  $\Pi = (\nabla \mathbf{u} + \nabla \mathbf{u}^T) - 2/3(\nabla \cdot \mathbf{u})$ . The scales chosen are the chamber radius  $a$ , the external poloidal magnetic flux  $\psi_0$  (from which the normalization factor for the magnetic field is obtained), and the Alfvén velocity  $c_A$ . Time is normalized with the Alfvén time  $\tau_A = a/c_A$ . The magnetic field and the current density have been further rescaled to absorb the constant  $\mu_0$ . The Reynolds and magnetic Reynolds numbers are  $Re = ac_A/\nu$  and  $Re_m = ac_A/\eta$ , where  $\nu$  is the kinematic viscosity, and  $\eta$  is the electrical resistivity. The

magnetic Reynolds number used in this work is  $Re_m = 10^5$ . The magnetic Prandtl number is set to one, i.e.,  $Re = Re_m$ .

The Equations (5) are solved in a uniform cartesian grid ( $N_x$ ,  $N_y$ , and  $N_z$ ) with  $N_x = N_y = 100$ , and  $N_z$  is proportional to the elongation. A high-resolution finite volume scheme based on a linearized Riemann solver for MHD was employed.<sup>28–30</sup> The total variation diminishing (TVD) condition of the solution was held using the Woodward limiter.<sup>31</sup> The  $\nabla \cdot \mathbf{B} = 0$  constraint was enforced using the projection method.<sup>32</sup>

Dirichlet boundary conditions are imposed for the normal component of the magnetic field (zero at  $r = 1$  and non-zero at the electrodes). In addition, we set  $\mathbf{j} \times \hat{n} = 0$  and use the no slip condition  $u = 0$ . Boundary conditions at the circular wall of the flux conserver are imposed using a high-order boundary treatment for regular grids.<sup>33</sup>

## B. Isolated configurations

As described in Section IID, when homogeneous boundary conditions are imposed, Eq. (1) leads to an eigenvalue problem. Each eigenvalue ( $k_l^n$ ) is proportional to the energy to helicity ratio of its corresponding eigenfunction, therefore, the plasma will evolve toward the state with the minimum of these eigenvalues, i.e., the relaxed state. In the case of a cylindrical domain, the relaxed state is axisymmetric provided that  $e < 1.67$ . For elongations above this value,  $k_1^{n=1}$  becomes smaller than  $k_1$  ( $n=0$  has been implicitly assumed), and thus, the relaxed state has an  $n=1$  dependence.<sup>11,12</sup>

To check if our scheme reproduces this behavior, we solved the system (5) inside a cylinder of elongation two, with vanishing normal fields at the boundary, using the axisymmetric state with  $\lambda = k_1$  as the initial condition. The analytic expression for these states can be found elsewhere.<sup>5</sup> The evolution of the magnetic configuration for  $e=2$  is shown in Fig. 9. In agreement with the previous studies, we observe that the system rapidly becomes unstable and evolves toward a completely tilted configuration. We note that the verification of the long term evolution towards the final minimum energy state was not performed in the previous works.<sup>11,12</sup>

To activate the instability, we applied a small and arbitrary  $n=1$  perturbation to the initial equilibria. Since the case  $e=2$  is well above the stability threshold, the exponential growth of the  $n=1$  mode was observed after a small

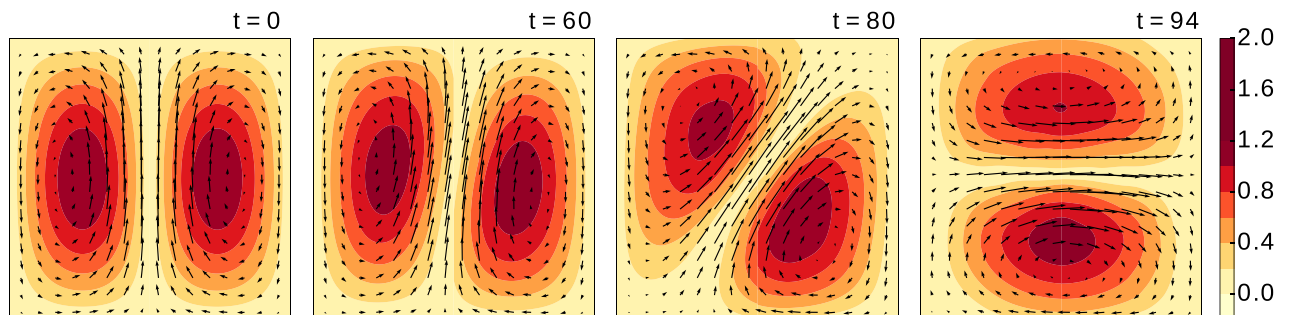


FIG. 9. Poloidal magnetic field (arrows) and toroidal magnetic field (colormap) showing the evolution of the tilt instability for  $e=2$ .



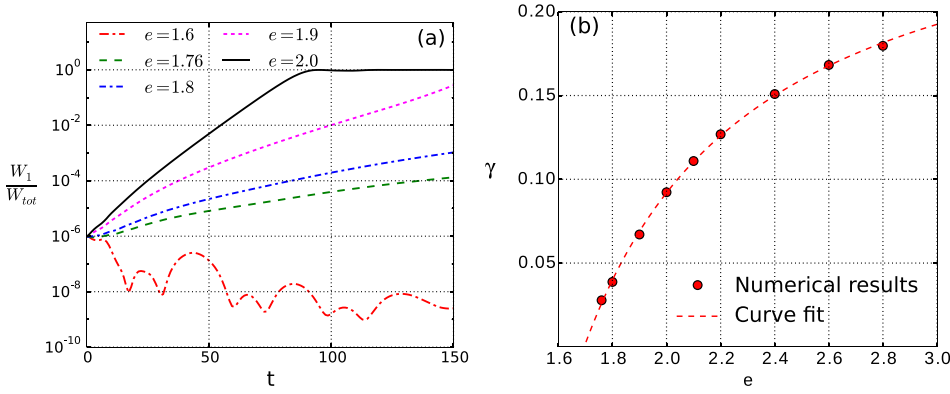


FIG. 10. (a) Evolution of the magnetic energy of the  $n=1$  mode ( $W_1$ ) relative to the total magnetic energy ( $W$ ) for isolated configurations with different elongations. (b) The growth rates obtained (points) are fitted and extrapolated to estimate the stability threshold ( $\gamma=0$ ).

transient. To eliminate this transient, the structure of the  $n=1$  mode during the phase of exponential growth was used as the perturbation in a new run. The process was repeated until the initial transient disappears, and the perturbation grew exponentially from  $t=0$ . In practice, a few restarts were required to obtain the correct tilt mode. The initial energy content of the perturbations was set to  $10^{-6}$  of the magnetic energy of initial condition. The evolution of the magnetic energy content of the  $n=1$  mode is shown in Fig. 10(a). In less than 100 Alfvén times, the magnetic energy of the system is completely transferred to the  $n=1$  mode.

The same procedure was applied to configurations with lower elongations, as shown in Fig. 10(a). As the elongation is reduced, the growth rate of the mode decreases, as expected. When values below the theoretical threshold 1.67 were used, the initial perturbation did not grow. Near this marginally stable situation, the estimation of small growth rates based on the time evolution of our non linear model becomes inaccurate. In order to improve the estimation of the stability threshold, the growth rates of unstable configurations were fitted and extrapolated. This procedure is shown in Fig. 10(b). The threshold elongation obtained in this way is 1.69, which is in reasonable agreement with the theoretical value.

### C. Effect of the open bias flux

When there is magnetic flux intercepting the boundary, Eq. (1) has the solution for any  $\lambda$ , excluding the eigenvalues. Since the description of ST-PCC plasmas was restricted to axisymmetric configurations, we were only able to capture the axisymmetric eigenvalues (i.e., a resonant behavior, see Figs. 2 and 3). We only consider regular configurations, thus  $\lambda < k_1$ . A further restriction on the maximum value of  $\lambda$  is imposed to prevent the tilt instability:  $\lambda < k_1^{n=1}$ . The latter condition becomes more restrictive for  $e > 1.67$  and imposes a limit on the maximum amplification factor attainable for each  $f$  (see Fig. 4). It is important to note that the preceding analysis is entirely based on the value of  $k_1^{n=1}$ , defined for isolated configurations. This means that this stability threshold does not take into account the effect of the external field lines tied to the electrodes.

To verify the scenario described above, based on the minimum energy (relaxation) principle, as well as to assess the improvement of stability produced by the external bias, we performed a series of simulations using the ST-PCC

configurations described by Eq. (3), as the initial condition. Three elongations were considered, namely, 2, 2.2, and 2.4. It is clear that, once the value of  $f$  is set, the equilibria will become unstable provided that  $\lambda$  (or equivalently  $\mathcal{A}$ ) is high enough. A stability threshold higher than  $k_1^{n=1}$  is expected due to line-tying stabilization.

Fig. 11 shows the growth rates obtained for three series of runs (one for each  $e$ ) when  $f=0.63$ . The abscissa was chosen to be  $\mathcal{A}$  (instead of  $\lambda$ ) for compatibility with the stability maps of Figs. 4 and 5. Each point was obtained following the same procedure that in Fig. 10(b) (see the explanation in Section III B). Again, extrapolation of the computed growth rates for unstable equilibria is used to estimate the stability boundary (a threshold in  $\mathcal{A}$ , in this case, that may also be expressed as a limit on  $\lambda$ ).

The threshold values obtained are plotted in Fig. 12 (points connected with dashed lines). The three zero-crossings of Fig. 11 give the three points at  $f=0.63$ . Note that each point in this plot corresponds to a family of runs. Solid lines indicate the stability limits deduced from the condition  $\lambda = k_1^{n=1}$  (as in Fig. 5). As expected, the simulations confirm the picture deduced from the minimum energy principle but predict a larger stable region due to the effect of the external bias. This effect produces a significant stability improvement for configurations with  $e=2$  and  $f$  in the range 0.7–0.9 and becomes less important for higher elongations and small values of  $f$ .

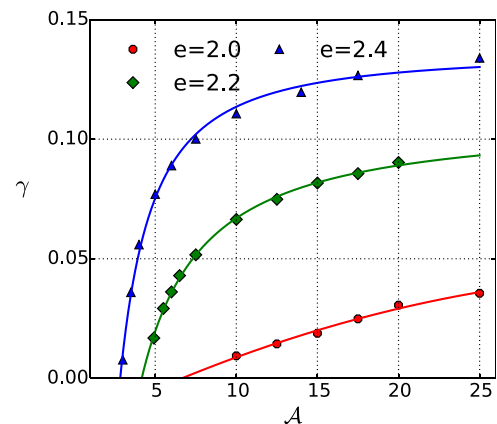


FIG. 11. Growth rates obtained for three series of runs with elongations 2, 2.2, and 2.4. The fraction of flux of the PCC is  $f=0.63$  in the three cases. Each point corresponds to one simulation.

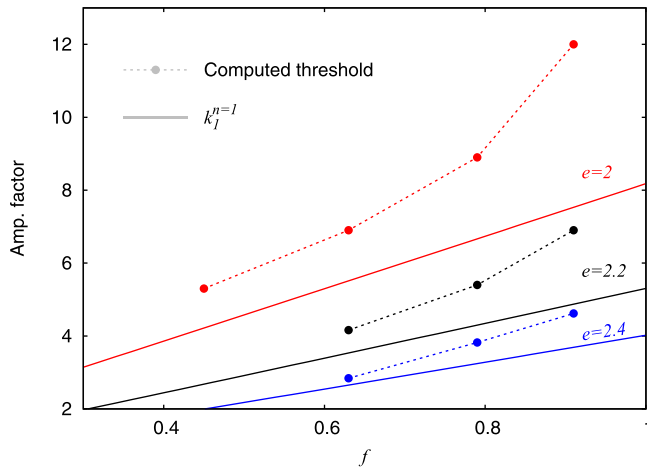


FIG. 12. Stability boundary predicted using the minimum energy principle (solid lines) compared to the computed stability threshold including the effect of the external flux (points and dashed lines). Note that each point corresponds to a family of simulations.

Finally, we point out that our study clarifies the double stabilizing role played by the central column. First, we showed that when the fraction of flux contained by the PCC increases, a larger  $\mathcal{A}$  can be achieved for the same  $\lambda$ . Since the tilt stability imposes a limit on  $\lambda$ , a central column with more flux allows for larger amplification factors below the threshold. This is a rather subtle and unexpected effect. Second, we confirmed the expected stabilizing effect of the line-tying at the electrodes and provided an estimation for it. Moreover, we showed that this effect is more pronounced for larger values of  $f$ , indicating that line-tying is more stabilizing at the PCC than at the CHI.

#### IV. CONCLUSIONS

The parameter space and stability of spherical tokamaks with a plasma center column have been studied. The mathematical statement of the equilibrium fields was given in terms of a Grad-Shafranov equation, and the role of the three relevant control parameters  $\lambda$ ,  $f$ , and  $e$  was clearly shown. Their impact on the main figures of merit of the equilibria, such as the flux amplification factor, the safety factor, and the aspect ratio, as well as on the stability to the tilt mode, was studied.

A first important conclusion of this study is that the effect of the vacuum bias flux on the equilibrium configuration essentially depends on a single quantity, namely,  $f$ , which gives the fraction of the external flux contained by the central column. We showed that the size of the electrodes and the flux distribution across them have only a minor impact on the equilibrium fields. Since  $f$  could in principle be varied for a given electrode set up (at least between different discharges), it turns out that it can be regarded as a relevant control parameter.

In particular, we showed that the flux amplification factor increases with  $f$  when  $\lambda$  is held constant.  $\lambda$  gives the normalized parallel current, is assumed to be spatially uniform (full relaxation hypothesis), and imposed by the electrostatic biasing of the electrodes. Therefore,  $(\lambda, f)$  can be regarded as

the *operation* control parameters defining the family of relaxed states with a given elongation. This clearly shows one of the additional degrees of freedom of the ST-PCC configuration, compared to the conventional CHI or flux core spheromaks.

The elongation is regarded as a *design* control parameter because it cannot be changed without modifying the geometry of the device. We observed, as expected, that the safety factor increases with  $e$ . Therefore, configurations with high elongations are desirable. However, the tilt mode becomes unstable for  $e > 1.67$ , in the absence of external bias flux.<sup>11,12</sup> When there is an external bias flux, on the other hand, stability is ensured provided that  $\lambda$  remains below the lowest non-axisymmetric eigenvalue of the homogeneous problem.<sup>4</sup> This criterion, based on the minimum energy principle, was graphically illustrated in the stability map of  $\mathcal{A}$  versus  $f$ . The region of tilt-stable relaxed states as well as the maximum amplification factor achievable for a given  $f$  and  $e$  are quickly deduced from these graphs.

A straightforward conclusion is that larger amplification factors can be achieved for larger values of  $f$ . This highlights a first, and rather subtle, stabilizing effect of the central flux column. The second stabilizing effect of the central column of flux is due to the field line-tying at the electrodes, as explained below. We also observed that the region of stable equilibria shrinks rapidly with the elongation. This suggests that configurations with  $e > 2.4$  may be of limited practical relevance.

The analysis presented so far is limited to the relaxed states of the ST-PCC configurations and does not take into account the line-tying of the external bias at the electrodes. In this work, we employed a non-linear MHD code to perform a dynamical stability analysis of the tilt mode including this effect. In the isolated case (no external bias), we observed that the code correctly reproduces the theoretical stability threshold ( $e = 1.67$ ). The threshold value was obtained by extrapolation of the growth rates for different elongations. In the presence of the external bias, the results are consistent with the stability criterion based on the minimum energy principle, but the stability thresholds are higher due to the effect of field line-tying at the electrodes. This effect produces a significant stability improvement for configurations with  $e \approx 2$  and  $f$  in the range of 0.7–0.9 but becomes less important for higher elongations and smaller values of  $f$ .

The use of a non-linear MHD code in the present work is justified as a desirable validation step in view of future studies of more complicated phenomena, such as the current and pressure driven modes, in this kind of configurations. We note that the same numerical scheme was successfully used in previous works to study the current driven instabilities<sup>13–15</sup> as well as the dynamics of formation and sustainment<sup>16,17</sup> of spheromak configurations.

#### ACKNOWLEDGMENTS

Financial support from UNCuyo Project 06/C431 is acknowledged.

- <sup>1</sup>Y.-K. Peng and D. Strickler, *Nucl. Fusion* **26**, 769 (1986).
- <sup>2</sup>Y.-K. M. Peng, *Phys. Plasmas* **7**, 1681–1692 (2000).
- <sup>3</sup>F. Alladio, P. Costa, A. Mancuso, P. Micozzi, S. Papastergiou, and F. Rogier, *Nucl. Fusion* **46**, S613 (2006).
- <sup>4</sup>X. Z. Tang and A. H. Boozer, *Phys. Plasmas* **13**, 42514 (2006).
- <sup>5</sup>J. B. Taylor, *Rev. Mod. Phys.* **58**, 741 (1986).
- <sup>6</sup>S. C. Hsu and X. Z. Tang, *J. Fusion Energy* **26**, 85 (2007).
- <sup>7</sup>S. O. Knox, C. W. Barnes, G. J. Marklin, T. R. Jarboe, I. Henins, H. W. Hoida, and B. L. Wright, *Phys. Rev. Lett.* **56**, 842 (1986).
- <sup>8</sup>M. G. Rusbridge, S. J. Gee, P. K. Browning, G. Cunningham, R. C. Duck, A. al-Karkhy, R. Martin, and J. W. Bradley, *Plasma Phys. Controlled Fusion* **39**, 683 (1997).
- <sup>9</sup>E. B. Hooper, R. H. Bulmer, B. I. Cohen, D. N. Hill, H. S. McLean, L. D. Pearlstein, C. A. Romero-Talamás, C. R. Sovinec, B. W. Stallard, R. D. Wood, and S. Woodruff, *Plasma Phys. Controlled Fusion* **54**, 113001 (2012).
- <sup>10</sup>J. B. Taylor, *Phys. Rev. Lett.* **33**, 1139 (1974).
- <sup>11</sup>J. M. Finn, W. M. Manheimer, and E. Ott, *Phys. Fluids* **24**, 1336 (1981).
- <sup>12</sup>A. Bondeson, G. Marklin, Z. G. An, H. H. Chen, Y. C. Lee, and C. S. Liu, *Phys. Fluids* **24**, 1682 (1981).
- <sup>13</sup>P. L. García Martínez and R. Farengo, *J. Phys.: Conf. Ser.* **16**, 012010 (2009).
- <sup>14</sup>P. L. García Martínez and R. Farengo, *Phys. Plasmas* **16**, 082507 (2009).
- <sup>15</sup>P. L. García Martínez and R. Farengo, *Phys. Plasmas* **16**, 112508 (2009).
- <sup>16</sup>P. L. García Martínez and R. Farengo, *Phys. Plasmas* **17**, 050701 (2010).
- <sup>17</sup>P. L. García Martínez, L. G. Lampugnani, and R. Farengo, *Phys. Plasmas* **21**, 122511 (2014).
- <sup>18</sup>T. R. Jarboe, I. Henins, A. R. Sherwood, C. W. Barnes, and H. W. Hoida, *Phys. Rev. Lett.* **51**, 39 (1983).
- <sup>19</sup>E. B. Hooper, L. D. Pearlstein, and R. H. Bulmer, *Nucl. Fusion* **39**, 863 (1999).
- <sup>20</sup>S. C. Hsu and P. M. Bellan, *Phys. Rev. Lett.* **90**, 215002 (2003), [arXiv:physics/0304104](https://arxiv.org/abs/physics/0304104).
- <sup>21</sup>C. R. Sovinec, J. M. Finn, and D. Del-Castillo-Negrete, *Phys. Plasmas* **8**, 475 (2001).
- <sup>22</sup>L. Woltjer, *Proc. Natl. Acad. Sci.* **44**, 489 (1958).
- <sup>23</sup>T. H. Jensen and M. S. Chu, *Phys. Fluids* **27**, 2881 (1984).
- <sup>24</sup>M. N. Rosenbluth and M. N. Bussac, *Nucl. Fusion* **19**, 489 (1979).
- <sup>25</sup>S. Chandrasekhar and P. C. Kendall, *Astrophys. J.* **126**, 457 (1957).
- <sup>26</sup>G. Toth, “A General Code for Modeling MHD Flows on Parallel Computers: Versatile Advection Code,” in *Magnetodynamic Phenomena in the Solar Atmosphere: Prototypes of Stellar Magnetic Activity* (Springer Netherlands, 1996) pp. 471–472.
- <sup>27</sup>P. L. Garcia-Martinez, in *Topics in Magnetohydrodynamics*, edited by L. Zheng (InTech, 2012) Chap. IV, pp. 85–116.
- <sup>28</sup>P. L. Roe, *J. Comput. Phys.* **43**, 357 (1981).
- <sup>29</sup>P. L. Roe and D. S. Balsara, *SIAM J. Appl. Math.* **56**, 57 (1996).
- <sup>30</sup>K. G. Powell, P. L. Roe, T. J. Linde, T. I. Gombosi, and D. L. de Zeeuw, *J. Comput. Phys.* **154**, 284 (1999).
- <sup>31</sup>P. Colella and P. R. Woodward, *J. Comput. Phys.* **54**, 174 (1984).
- <sup>32</sup>G. Toth, *J. Comput. Phys.* **161**, 605 (2000).
- <sup>33</sup>H. Forrer and R. Jeltsch, *J. Comput. Phys.* **140**, 259 (1998).